PNAS RESEARCH ARTICLE | EARTH, ATMOSPHERIC, AND PLANETARY SCIENCES

Sea ice fluctuations in the Baffin Bay and the Labrador Sea during glacial abrupt climate changes

Federico Scoto[a,b,1], Henrik Sadatzki[c], Niccolò Maffezzoli[b,d], Carlo Barbante[b,d], Alessandro Gagliardi[e], Cristiano Varin[b], Paul Vallelonga[f], Vasileios Gkinis[f], Dorthe Dahl-Jensen[f,g], Helle Astrid Kjær[f], François Burgay[b,h], Alfonso Saiz-Lopez[i], Ruediger Stein[c,j], and Andrea Spolaor[b,d,1]

Edited by Julie Brigham-Grette, University of Massachusetts Amherst, Amherst, MA; received February 25, 2022; accepted September 3, 2022 by Editorial Board Member Akkihebbal R. Ravishankara

Sea ice decline in the North Atlantic and Nordic Seas has been proposed to contribute to the repeated abrupt atmospheric warmings recorded in Greenland ice cores during the last glacial period, known as Dansgaard-Oeschger (D-O) events. However, the understanding of how sea ice changes were coupled with abrupt climate changes during D-O events has remained incomplete due to a lack of suitable high-resolution sea ice proxy records from northwestern North Atlantic regions. Here, we present a subdecadal-scale bromine enrichment (Br_{enr}) record from the NEEM ice core (Northwest Greenland) and sediment core biomarker records to reconstruct the variability of seasonal sea ice in the Baffin Bay and Labrador Sea over a suite of D-O events between 34 and 42 ka. Our results reveal repeated shifts between stable, multiyear sea ice (MYSI) conditions during cold stadials and unstable, seasonal sea ice conditions during warmer interstadials. The shift from stadial to interstadial sea ice conditions occurred rapidly and synchronously with the atmospheric warming over Greenland, while the amplitude of high-frequency sea ice fluctuations increased through interstadials. Our findings suggest that the rapid replacement of widespread MYSI with seasonal sea ice amplified the abrupt climate warming over the course of D-O events and highlight the role of feedbacks associated with late-interstadial seasonal sea ice expansion in driving the North Atlantic ocean–climate system back to stadial conditions.

sea ice reconstruction | Baffin Bay | Labrador Sea | abrupt climate changes | Dansgaard-Oeschger events

Significance

Dansgaard-Oeschger (D-O) events are abrupt atmospheric warming events in Greenland that occurred repeatedly during the last glacial period. Combining proxy records from an ice core and a sediment core, we reconstruct sea ice conditions in the Baffin Bay and the Labrador Sea during several D-O events between 34 and 42 thousand years ago. Our results reveal in detail that widespread sea ice decline was synchronous with the atmospheric warming of the D-O events, highlighting the importance of sea ice decline in amplifying abrupt high-latitude climate warming. We also find re-expansion of seasonal sea ice during the late phase of warm interstadial periods, which likely contributed to a feedback loop in the sub-polar North Atlantic driving the climate system back to cold stadial conditions.

The Dansgaard-Oeschger (D-O) cycles imprinted in Greenland ice core records are millennial-scale climate fluctuations between cold Greenland stadial (GS) periods and warmer Greenland interstadial (GI) periods, that occurred at least 25 times during the last glacial cycle (1–3). Each D-O event is characterized by an abrupt atmospheric warming over Greenland by up to ∼15°C within a few decades, followed by a gradual cooling lasting for 1–2 ka and a final temperature drop that marks the beginning of a new GS period (3–7). Although various climate proxy records from both hemispheres document fluctuations of the Earth's glacial climate (8), the ultimate triggers and mechanisms of the millennial-scale D-O climate changes are still not fully understood. Hypotheses explaining the abrupt D-O climate transitions in the Northern Hemisphere often include a rapid sea ice decline in the North Atlantic Ocean and the Nordic Seas (9–11). Sea ice decline, in turn, may have triggered critical climate feedbacks that amplified the regional-to-hemispheric atmospheric warming, analogous to what is observed today in some Arctic regions (12, 13). Before the so-called satellite-era, however, our understanding of past Arctic sea ice regimes is very limited and relies on a few semiquantitative proxy reconstructions from sediment and ice core records (14–16). The former are based on the assemblage of sea ice-associated organisms and their organic biomarkers in marine sediments (17–20), while, among the sea ice markers from ice core archives, the bromine-to-sodium ratio (referred to as bromine enrichment; Br_{enr}) is commonly associated with seasonal sea ice conditions in the aerosol entrainment area (21).

To reconstruct the glacial sea ice variability in the Nordic Seas, previous studies have combined biomarker data from sediment cores retrieved in the Norwegian Sea with Br_{enr} data from the East Greenland RECAP (Renland Ice Cap Project) ice core (9, 10, 22). The combined sea ice records suggest a millennial-scale variability over the glacial D-O cycles with an extensive seasonal sea ice cover (or first-year sea ice; FYSI) during colder GS and more pronounced open-ocean conditions during warmer GI (9, 10, 22, 23). Extensive and rapid sea ice reduction in the Nordic Seas may have happened within 250 y or less, concomitant with reinvigoration of deep convection and the abrupt warming transitions in Greenland (9, 10). On the other hand, the Br_{enr} record from the NEEM

Author contributions: F.S., H.S., C.B., P.V., A.S.-L., and A.S. designed research; F.S., H.S., N.M., C.B., A.G., C.V., P.V., D.D.-J., F.B., A.S.-L., R.S., and A.S. performed research; F.S., H.S., N.M., C.B., A.G., C.V., P.V., V.G., D.D.-J., H.A.K., F.B., A.S.-L., R.S., and A.S. analyzed data; and F.S., H.S., N.M., C.B., A.G., C.V., P.V., V.G., D.D.-J., H.A.K., F.B., A.S.-L., R.S., and A.S. wrote the paper.

The authors declare no competing interest.

This article is a PNAS Direct Submission. J.B.-G. is a guest editor invited by the Editorial Board.

[1]To whom correspondence may be addressed. Email: federico.scoto@unive.it or andrea.spolaor@unive.it.

This article contains supporting information online at http://www.pnas.org/lookup/suppl/doi:10.1073/pnas.2203468119/-/DCSupplemental.

Published October 24, 2022.

(North Greenland Eemian Ice Drilling) ice core has been used to reconstruct the sea ice evolution in the Canadian Arctic and Baffin Bay over the last glacial cycle (130 ka to present) (24). Specifically, lower Br_{enr} values observed in the NEEM ice core during GS have been interpreted with a widespread multiyear sea ice (MYSI) cover, while higher Br_{enr} values during GI have been associated with enhanced FYSI conditions (24). The temporal resolution of the previously published glacial NEEM record (~60–120 y), however, did not allow any detailed investigation of sea ice changes during the D-O climate cycles or its temporal relationship with the atmospheric warming.

Here we present a subdecadal record of NEEM Br_{enr} to reconstruct the sea ice variability in the Baffin Bay during D-O events 7–10 that occurred between 34 and 42 ka (b2k = before 2000 CE). To enhance the interpretation and spatial coverage of our sea ice reconstruction, we compare the NEEM Br_{enr} sea ice record with an independent marine biomarker sea ice record from the Eirik Drift off South Greenland that reflects sea ice changes in the northern Labrador Sea. This study provides unprecedentedly detailed insights into millennial-scale and shorter-term sea ice fluctuations in regions west and south of Greenland during times of abrupt climate changes.

Results

Core Sites, Chronology, and Sea Ice Proxies. The 2,540 m-long NEEM ice core retrieved in North West Greenland between 2008 and 2012 (77°45' N, 51°07' W, 2,479 m a.s.l.; Fig. 1) preserves a comprehensive record of the Greenland climate since the last interglacial, the Eemian (130 ka) (). At present, the mean annual temperature at the ice core site is −29 °C and the accumulation rate is 0.22 m ice equivalent/year (25). The dating of the NEEM ice core was done according to the GICC05modelext-NEEM-1 age scale (26). The source region of marine aerosols and bromine deposited at the NEEM site encompasses the Canadian Archipelago, the Hudson Bay, and the Baffin Bay (24, 27), regions that are today mostly covered by seasonal sea ice (28). However, empirical and modeling evidence (29–32) suggest that the Laurentide Ice Sheet over North America also extended over the Canadian Archipelago and the Hudson Bay during the last glacial maximum (~24 ka). On the contrary, the Baffin Bay was probably covered by perennial sea ice but not by an ice sheet (33). We therefore assume that the glacial NEEM Br_{enr} profile might largely reflect sea ice changes in the Baffin Bay area.

To discriminate between perennial vs. seasonal sea ice regimes and to evaluate the overall temporal sea ice response to glacial D-O events, we employ subdecadal records of bromine and sodium alongside stable oxygen isotopes data [$\delta^{18}O$ (34)] (Figs. 2 and 3). Both records are obtained from the subsampling of the NEEM ice core between 1,711 and 1,793 m depth that corresponds to a time interval between 34 and 42 ka. This period encompasses four D-O cycles (D-O 7–10), including Heinrich event 4 (HE4) (35).

The NEEM high-resolution discrete samples (2–3 cm) were collected only in proximity of each D-O transitions (*SI Appendix, Materials and Methods*). We filled the measurement gaps for Br and Na records with low-resolution (110 cm) data from a previous study (24). NEEM $\delta^{18}O$ and accumulation rate data were obtained through Continuous Flow Analysis (34, 36).

The Br_{enr} sea ice proxy is calculated from the bromine-to-sodium mass ratio measured in the ice samples normalized to that of bulk seawater (where $[Br]/[Na]_{seawater} = 0.0062$ (37)). The primary mechanism that leads to increased Br_{enr} values in polar ice is the auto-catalytic release of bromine species from sea ice saline substrates into the polar boundary layer during springtime, which eventually results in bromine-enriched snow deposited at the ice core site (21, 38–40). Increased levels of Br_{enr} are hence associated with seasonal, or first-year, sea ice conditions in the ice core source region of aerosol (11, 21, 22, 40–45) (*SI Appendix, Materials and Methods*), while the $\delta^{18}O$ record is commonly used as an indicator of local atmospheric temperatures (5, 34, 46, 47).

We complement our Br_{enr} sea ice record with a biomarker-based sea ice proxy record from the Eirik Drift core GS16-204–23CC (58°13' N, 45°42' W, Fig. 1), which allows us to constrain shifts of the glacial sea ice edge south of Greenland during the D-O cycles. Biomarkers were analyzed in samples from the interval between 341 and 560 cm core depth, corresponding to the time interval between 31 and 42 ka. The sea ice biomarker IP_{25}, a highly branched isoprenoid (HBI) monoene, is used to trace the occurrence of seasonal sea ice (17), brassicasterol as a tracer for open water conditions (18), and the HBI triene (HBI-III) to identify the retreating sea ice edge or marginal ice zone (19, 20). The age model for the section investigated in core GS16-204–23CC is based on stratigraphic alignment of its magnetic susceptibility record to that of nearby core JPC15, and tuning of the relative paleointensity record of JPC15 to that of the well-dated core PS2644, whose age model is based on a tuning to the GICC05 chronology but is independently supported by numerous foraminiferal ^{14}C ages and tephra layers (48). The age model and the temporal resolution of our biomarker records of core GS16-204–23CC sufficiently constrain and resolve the sea ice conditions during stadial and interstadial periods between GS-7 and GS-9, allowing for a comparison to and supporting the NEEM ice core records at least on a millennial time scale. The sediment core chronology and methodology are detailed in the *SI Appendix, Materials and Methods*.

Baffin Bay Sea Ice Conditions during Abrupt Glacial Climate Changes. Between 34 and 42 ka, both NEEM sodium and bromine concentrations display a millennial-scale variability strictly in anti-phase with the NEEM $\delta^{18}O$ temperature proxy profile and with about a 3-fold increase during GS compared to warmer GI (Fig. 2 *A*, *D*, and *E*). Sodium stadial/interstadial variability has been primarily explained by a change in accumulation and/or in wind strength (36) (Fig. 2*B*).

Similarly, although bromine concentrations are generally higher during GS, we note increased levels over the course and/or in the final phase of GI (Fig. 2*E*). This may be associated with a change in the seasonality of precipitation (49, 50), and/or more extended seasonal sea ice in the Baffin Bay, the latter leading to an extra source of inorganic bromine deposited at NEEM (24, 42). As previously mentioned, it is important to remark that each D-O climate cycle involved substantial changes both in atmospheric temperature (4, 26) and wind patterns (6, 36), as well as precipitation with almost doubled snow accumulation rate during the GI compared to the GS periods (Fig. 2*B*) (26, 51). Nevertheless, we observe that also the calculated sodium and bromine deposition fluxes do not show any substantial differences with respect to the trends in elemental concentrations (*SI Appendix*, Fig. S2).

In line with the previous long-term Br_{enr} reconstruction (24), each GS-GI transitions is marked by an increase of Br_{enr} mean-value concomitant with the $\delta^{18}O$ shifts, suggesting a close link between the rapid atmospheric warmings over Greenland and increased seasonal sea ice conditions in the Baffin Bay (24) (Fig. 3 *A* and *B* and Table 1). In particular, the highest Br_{enr} mean values occur during the long-lasting and more

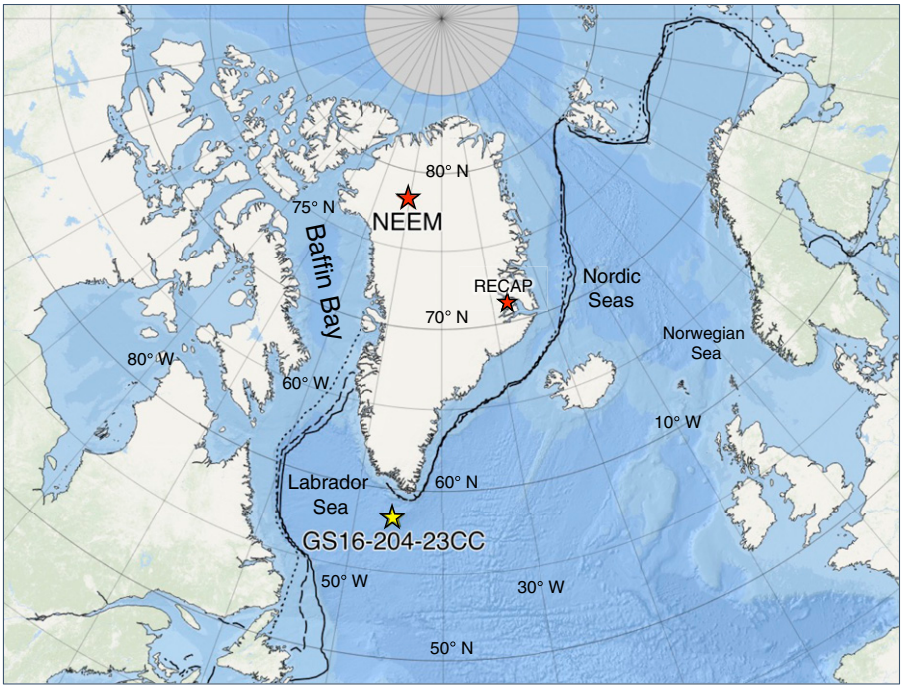

Fig. 1. Overview of the location sites of ice and marine sediment cores used in this study. Red stars indicate the NEEM and RECAP ice cores locations. Yellow star indicates the marine sediment core GS16-204–23CC. Black lines mark the median sea ice edge position during March (solid), April (dashed), May (dotted) averaged over the period 1981–2010 (https://nsidc.org) (65). The map was produced with QGIS (*v3.10.10*).

pronounced interstadials such as GI-8 [Br_{enr} = 3.52 ± 4.29 (1σ); duration = 1,640 y (51)], GI-10 [Br_{enr} = 2.91 ± 2.87 (1σ); duration = 660 y (51)], and GI-7 [Br_{enr} = 2.75 ± 3.80 (1σ); duration = 740 y (51)], when the reconstructed temperature increase (ΔT) at the NEEM site was between 7 and 9°C (4) (Table 1). In contrast, a smaller increase in Br_{enr} mean value is observed during the shortest and less intense event GI-9 [Br_{enr} = 2.28± 2.07 (1σ); duration = 260 y (51); ΔT= ∼6°C (4)], indicating a less extensive seasonal sea ice cover in the Baffin Bay compared to the other GI (Table 1). In relative terms, the highest increase of mean-Br_{enr} with respect to the previous stadial period occurs during GI-8 (+52%), followed respectively by GI-10 (+35%), GI-7 (+31%), and GI-9 (+7%).

Taken at face value, the relative increase of Br_{enr} mean value between stadial and interstadial periods (Table 1) might indicate an overall limited-to-moderate expansion of the total seasonal sea ice cover in the Baffin Bay. However, focusing on the internal (subdecadal) GS/GI Br_{enr} variability, thus taking into account the SD of Br_{enr} data, σ, we can clearly identify a significant change at the onset of each D-O event (Table 1 and *SI Appendix*, Fig. S3). We suggest that the combined increase of both absolute Br_{enr} mean values and its associated SD can be used as a proxy of sea ice stability during the glacial abrupt D-O cycles. Indeed, a lowered σ during stadial periods ($Br_{enr\ GS}$ = 2.21 ± 0.81 [1σ], excluding GS-7 of which we do not have the complete D-O cycle) supports the hypothesis of a stable, widespread MYSI cover over the Baffin Bay and limited FYSI fluctuations. In contrast, the concurrent increase of Br_{enr} mean value and its associated SD during the interstadial periods ($Br_{enr\ GI}$ = 2.97 ± 3.63 [1σ]) is reflective of more unstable sea ice conditions characterized by a reduced MYSI cover and more pronounced FYSI variability.

Timing of Baffin Bay Sea Ice Changes with Respect to D-O Climate Events. Isotope-enabled model simulations of D-O-type events have demonstrated that, especially for long lasting events, the $\delta^{18}O$ variability in southern Greenland ice cores can be nearly entirely explained by sea ice changes (46). In northern Greenland and in particular at the NEEM site, however, the impact of sea ice loss on the water isotopes profile has been suggested to be of secondary importance (46). In this context, NEEM $\delta^{18}O$ and Br_{enr} records are, to some extent, relatively independent of each other with the former capturing the abrupt near-surface air temperatures variations and the latter reflecting different sea ice conditions.

To assess the temporal relationship between the abrupt Greenland atmospheric warmings and the glacial Baffin Bay sea ice change, we employ a statistical analysis to define a) the D-O onset based on structural changes in the $\delta^{18}O$ series and b) the first occurrence of a statistically significant increase of the Br_{enr} variability (*SI Appendix, Materials and Methods*). We hence calculate the Baffin Bay sea ice time response as the time interval between the D-O onset and the first statistically significant change in the variability of the Br_{enr} sea ice proxy *(SI Appendix, Materials and Methods)*. Table 2 shows that, except for D-O 7 (where there is a lead of 9 y), during all the other D-O events considered, the first significant change of Br_{enr} variability is coeval with the $\delta^{18}O$ shifts, suggesting a synchronous sea ice response to glacial abrupt climate warmings.

Based on the subdecadal temporal resolution of the NEEM ice core samples [2–6 y for Br_{enr} and 2–8 y for $\delta^{18}O$ (34)], we argue that the breakup of the near-perennial sea ice cover and the shift to more seasonal sea ice conditions in the Baffin Bay might have happened conservatively within one decade at the D-O onset. Although we do not resolve the causal relationship between the two climatic components, we find that the Br_{enr} variability steadily increases when the NEEM $\delta^{18}O$ exceeds ∼−42 ± 1‰ (95% confidence interval) and it decreases below this threshold value (yellow band in Fig. 4*A* and *SI Appendix, Materials and Methods*). This result highlights a quantitative link between past Baffin Bay sea ice stability and glacial abrupt climate variability, which might be

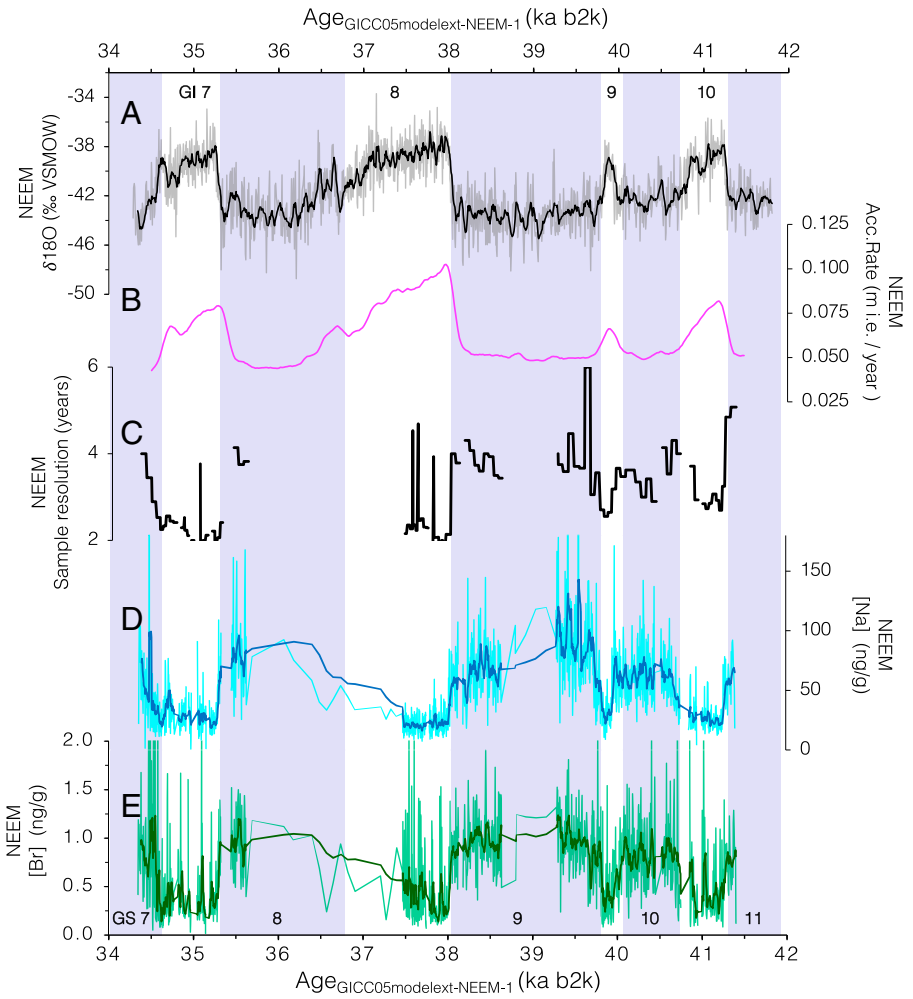

Fig. 2. NEEM stable oxygen isotopes, bromine, and sodium variability over D-O events 7–10. (*A*) Subdecadal $\delta^{18}O$ (thin line) with 10-points moving average (thick line) (34); (*B*) NEEM snow accumulation rate (magenta) (36); (*C*) temporal resolution of the novel NEEM sodium and bromine data presented in this study; (*D*) sodium and (*E*) bromine concentrations (thin lines) with 10-points moving average (thick lines). Gaps of sodium and bromine data longer than 50 y are filled with lower resolution data from a previous study (24). The chronology is the GICC05modelext-NEEM-1 timescale (26). Shaded bars indicate the GS, which are numerated at the *Bottom* while white bands indicate GI numerated at the *Top*.

tested as a constraint for glacial coupled atmospheric-sea ice model simulations.

Furthermore, we use a spline to smooth the squared deviations from the mean of Br_{enr} in order to assess the temporal evolution of the Baffin Bay sea ice changes during the selected D-O cycles (Fig. 4 and *SI Appendix, Materials and Methods*). The smoothed curves of the squared deviations of Br_{enr} follow the $\delta^{18}O$ glacial climate variability, with lower values associated with a stable MYSI regime and higher values suggesting enhanced FYSI conditions (Fig. 4*C*). Yet, we observed that the maxima of the smoothed curves of Br_{enr} squared deviations, interpreted as the most pronounced sea ice fluctuations, are not synchronous with the abrupt atmospheric warmings displayed by $\delta^{18}O$, but delayed by up to several centuries with respect to the D-O onsets (Fig. 4, red dashed lines). The smoothed squared deviations of Br_{enr} values during D-O 7 suggest that the most pronounced variation of the reconstructed Baffin Bay FYSI cover occurs ~0.7 ka after the D-O onset, coinciding approximately with the termination of GI-7. Similarly, the most variable FYSI conditions during D-O events 8 and 10 are attained ~0.4 ka and 0.25 ka after the onsets of GI-8 and GI-10, respectively. For the shortest and less intense D-O 9, the time lag is only 70 y. (Fig. 4*C* and Table 2). We note that the longest response times for most variable sea ice conditions being reached after the onsets of D-O events 8 and 7 were also accompanied by the largest amplitudes of the interstadial sea ice fluctuations. We argue that the short-term sea ice fluctuations increased in amplitude through GI, with their maximum being reached near the end of the GI, but were substantially muted during GS.

Sea Ice Proxy Evidence from the Eirik Drift Sediment Core. Biomarker records of core GS16-204–23CC are used to reconstruct the stadial and interstadial sea ice conditions in the Labrador Sea south of Greenland, extending our ice-core-based sea ice reconstruction for the Baffin Bay. This core site is today located under annually ice-free conditions, just south of the East Greenland Current extension that transports cold and ice-laden waters around the southern tip of Greenland into the Labrador Sea (Fig. 1). It is thus ideally suited to trace a potentially enhanced and variable sea ice cover and/or export in the northwestern North Atlantic during abrupt D-O climate changes.

To investigate the past sea ice conditions and phytoplankton production, we used IP_{25}, a monounsaturated HBI with 25 carbon atoms, the triunsaturated HBI-III, and brassicasterol. IP_{25} is produced by certain sea ice diatoms and found in increased abundance in surface sediments underlying a seasonal sea ice cover in Arctic and sub-Arctic regions (17, 52, 53). In turn, it is (almost)

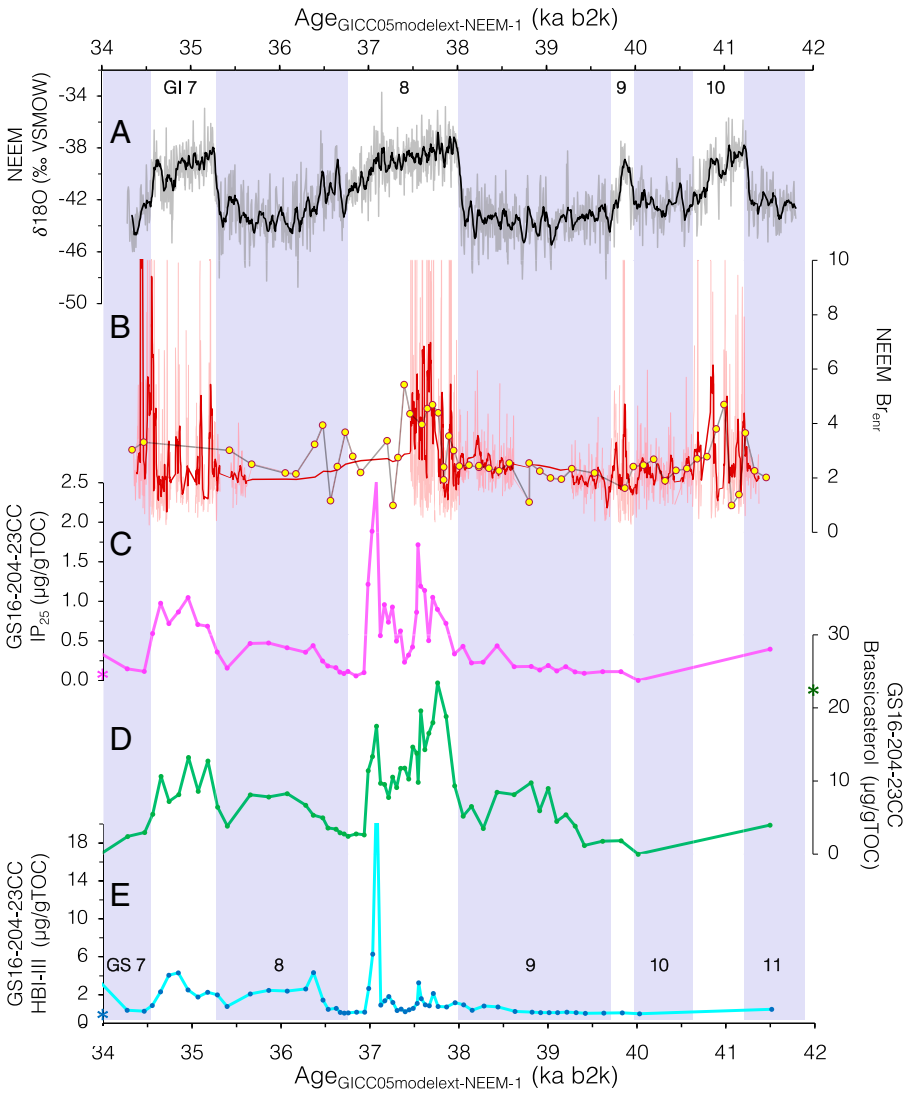

Fig. 3. Stable oxygen isotopes and bromine enrichment from NEEM and biomarker proxy records from the Eirik Drift (Labrador Sea). (*A*) Subdecadal $\delta^{18}O$ (thin line) with 10-points moving average (thick line) (34); (*B*) NEEM bromine enrichment (thin line) with 10-points moving average (thick line) and low-resolution data from a previous study (yellow dots) (24). (*C*) GS16-204–23CC record of IP_{25} (magenta), (*D*) brassicasterol (green), and (*E*) HBI-III (light blue). Asterisks indicate GS16-204–23MC core-top values for comparison (10, 53). The chronology is the GICC05modelext-NEEM-1timescale (26). Shaded bars indicate the GS, which are numerated at the *Bottom* while white bands indicate GI numerated at the *Top*.

absent in surface sediments underlying either a perennial sea ice cover or an ice-free, open ocean. HBI-III is produced by open-water diatoms especially in the marginal ice zone, while brassicasterol is formed by diatoms and other phytoplankton in the open ocean (17, 18, 20). Both biomarkers are found in sediments underlying open-ocean conditions and under the seasonally retreating sea ice edge, but are largely absent under (near-)perennial sea ice (20, 52, 53). Biomarker data from Eirik Drift core-top samples, including that of the core site investigated here, show increased brassicasterol concentrations and decreased IP_{25} and HBI-III concentrations relative to downcore (13), reflecting the modern open-water conditions south of Greenland (Fig. 3 *C*–*E*).

The biomarker records of core GS16-204–23CC show concentrations of 0–2.5 µg/gOC for IP_{25}, 0–6.3 µg/gOC for HBI-III (in one sample up to 24.7 µg/gOC), and 0–23.4 µg/gOC for brassicasterol, with all biomarkers varying largely in parallel throughout the record between ∼31–42 ka (Fig. 3 *C*–*E* and *SI Appendix*, Fig. S4). IP_{25}, HBI-III, and brassicasterol are low over large parts of the record, in particular during stadials, while increased biomarker abundances are observed in two intervals that correspond to GI-8 and GI-7. An interstadial increase in biomarker values is not resolved for the other shorter-lasting GI, possibly because of the temporal resolution of the records being too low (*SI Appendix*, Fig. S4). While the core-top of the core site investigated here shows elevated brassicasterol and substantially reduced IP_{25} and HBI-III concentrations (Fig. 3 *C*–*E*), the stadial and interstadial biomarker signals in core GS16-204–23CC resemble biomarker values observed in core-tops from the perennially ice-covered and seasonally ice-covered East Greenland margin, respectively (10). The contemporaneously increased abundance of IP_{25} and brassicasterol in core GS16-204–23CC thus suggests an enhanced sea ice algae and phytoplankton production under a seasonal sea ice cover. This is also consistent with increased HBI-III values that may indicate a seasonally retreating sea ice edge or marginal ice zone conditions over the core site during interstadials. By contrast, extremely reduced IP_{25}, HBI-III, and brassicasterol values suggest a reduction in both sea ice algae and open-water phytoplankton production, which we interpret as reflecting a more extensive, near-perennial sea ice cover during stadials.

The biomarker-based sea ice record of GS16-204–23CC reflects both generally enhanced sea ice conditions between

Table 1. Bromine enrichment mean values during D-O events 7–10

Stadial					Interstadial					
	N. sample	Average	σ	SE		N. sample	Average	σ	SE	ΔT (°C)
GS-7	52	4.48	10.68	1.48	**GI-6**	–	–	–	–	–
GS-8	72	2.09	0.72	0.08	**GI-7**	247	2.75	3.80	0.24	–
GS-9	246	2.31	0.83	0.05	**GI-8**	233	3.52	4.29	0.28	**+ 8.85**
GS-10	172	2.14	0.84	0.06	**GI-9**	91	2.28	2.07	0.22	**+ 6.02**
GS-11	31	2.16	0.52	0.09	**GI-10**	160	2.91	2.87	0.23	**+ 7.72**
All GSs	573	2.42	3.34	0.14	**All GIs**	731	2.97	3.63	0.13	–
All GSs* (no GS-7)	521	2.21	0.81	0.04						

The last column (ΔT) shows the reconstructed temperature difference during each GS/GI transition (4).

34 and 42 ka, as compared with modern ice-free conditions, and glacial sea ice reductions during GI-7 and GI-8. Hence, our combined sea ice records from the NEEM ice core and the Eirik Drift sediment core indicate that an extensive MYSI cover prevailed in both the Baffin Bay and in the northern Labrador Sea during stadials and that seasonal sea ice conditions characterized both regions west and south of Greenland during interstadials. As the sea ice cover south of Greenland is largely influenced by drift ice originating from the East Greenland Current and transported around the southern tip of Greenland into the Labrador Sea, the biomarker data of core GS16-204–23CC may also indicate that sea ice export into the subpolar North Atlantic was generally enhanced during the glacial and particularly during stadials, as compared to modern conditions. The fact that IP_{25} and other biomarkers in core GS16-204–23CC show two successive peaks in the early and late phases of GI-8 (Fig. 3 *C–E*) may reflect northward and southward shifts of the sea ice edge and/or changes of sea ice export over the core site. This would imply the presence of an interstadial turning point at which the system switched from sea ice retreat to sea ice expansion, similar to the findings from the NEEM Br_{enr} record.

Discussion

The glacial NEEM Br_{enr} ice core record with increased chronological resolution between 34 and 42 ka, complemented by biomarker records from the Eirik Drift, allows an unprecedented view of glacial sea ice dynamics south and west of Greenland during times of abrupt climate change.

The last glacial cycle is characterized by significantly low NEEM Br_{enr} values (Br_{enr} ~2–4), confirming the presence of an extensive near-perennial sea ice cover over the Canadian Arctic and Baffin Bay with the FYSI bromine-source located far south of the NEEM site (6, 24, 46) (Fig. 5*A*). During the D-O cycles considered, NEEM Br_{enr} mean values are generally lower during stadial periods compared to the subsequent interstadials, suggesting prevailing MYSI conditions in the NEEM aerosols source area. Peculiarly, although we have no available data from the next GI-6 for comparison, we do observe the highest Br_{enr} mean value during GS-7 ($Br_{enr\ GS\text{-}7}$= 4.48; Table 1) explained by two single data points (Br_{enr} = 78.2 and 15.2, respectively). Excluding the two outliers*, in fact, the mean $Br_{enr\ GS\text{-}7^*}$ decreases to 2.79.

Conversely to stadial periods, long-lasting interstadials like GI-8 and GI-7 show a relative increase of Br_{enr} in the NEEM ice core accompanied by higher levels of IP_{25}, HBI-III, and brassicasterol in the GS16-204–23CC sediment core, suggesting overall enhanced seasonal sea ice conditions.

This in turn implies a loss of the prevalent perennial cover and a partial replacement by seasonal sea ice in both the Baffin Bay and northern Labrador Sea. The extensive FYSI conditions originated by the retreat of the MYSI edge support enhanced springtime inorganic bromine recycling on the seasonal sea ice surface (21, 44) with subsequent increase of Br_{enr} levels at the NEEM site (Fig. 5*B*).

The shift from extensive MYSI to rather FYSI in the Baffin Bay and the Labrador Sea in response to each GS-GI transitions is in agreement with a reinvigoration of the AMOC and an associated increase in northward surface ocean heat transport to the subpolar North Atlantic (54, 55). Reduced, seasonal sea ice conditions reflected in our records for GI-7 and 8 suggest that at least partially ice-free conditions in the Labrador Sea may have been associated with open-ocean convection and deep-water formation in that region. Consistent with model simulation of the glacial climate variability, sea ice retreat and increased deep-water formation in the Labrador Sea might have contributed to a strengthened AMOC during GI (56). On the other hand, extensive near-perennial sea ice conditions in the Baffin Bay and Labrador Sea during GS and associated enhanced sea ice export to the subpolar North Atlantic, where (seasonal) sea ice melting would lead to a surface freshening, argue for suppressed local deep ocean convection in agreement with a reduced AMOC.

Table 2. Year (b2k) of the first significant change of NEEM Br_{enr}

D-O event	GI onset NEEM δ18O (year b2k)	Br_{enr} onset NEEM Br_{enr} (year b2k)	Max Br_{enr}SSD (year b2k)	Delta (NEEM GI onset − max Br_{enr} SSD) (years)
7	35,473	35,464	34,780	693
8	38,214	38,214	37,821	393
9	40,134	40,134	40,064	70
10	41,448	41,448	41,198	250

The first column shows the year (b2k) of the GI onsets defined from the structural changes in the NEEM $\delta^{18}O$ record. The second column show the year (b2k) of the first significant change of the Br_{enr} profile. The third column displays the year of maxima smoothed squared deviations (SSD) of Br_{enr}. The last column reports the time interval (Delta) between the NEEM GI onset and the maxima of SSD.

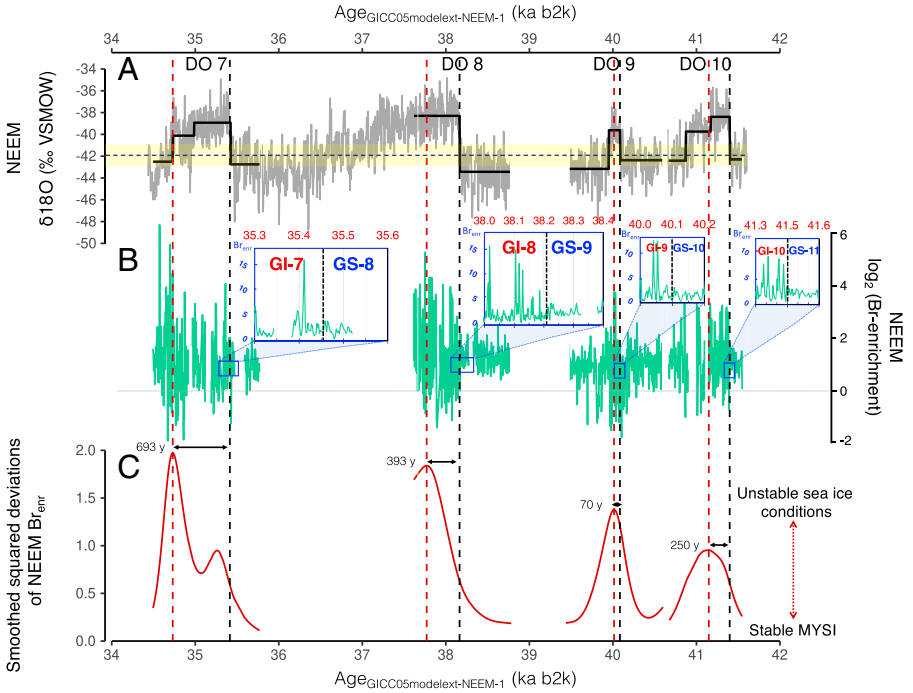

Fig. 4. NEEM stable oxygen isotopes and bromine enrichment variability across D-O 7–10. (*A*) Black segments indicate the estimated structural changes in the $\delta^{18}O$ series; (*B*) NEEM Br_{enr} data plotted on a log2 scale with blown-up views centered on each stadial/interstadial transition plotted on a normal scale; (*C*) smoothed squared deviations from the mean of Br_{enr} series. The black vertical dashed lines indicate the onset of each D-O event using NEEM $\delta^{18}O$ data (*SI Appendix, Materials and Methods* for more details) while the red vertical dashed lines indicate the maxima of the smoothed squared deviations from the mean of Br_{enr}. The chronology is the GICC05modelext-NEEM-1 timescale (26).

The glacial millennial-scale sea ice changes reconstructed for the Baffin Bay and the northern Labrador Sea are generally consistent with those reconstructed for the Nordic Seas. While sea ice reductions in the Nordic Seas were found to have occurred within 250 y or less at or just before the onset of a D-O event (9, 10), our data indicate that the breakup of the perennial sea ice cover and the shift to increased seasonal sea ice conditions west and south of Greenland occurred within a decade and synchronously with the D-O climate warming transitions. The tight coupling between sea ice changes and Greenland temperature changes during the D-O cycles and their nonlinear climate transitions (7) is further illustrated by the threshold behavior that we identified between changes in Br_{enr} and $\delta^{18}O$ of the NEEM ice core (Fig. 4*A*). Our results thus support hypotheses that invoke rapid and widespread sea ice decline and associated feedbacks in subpolar North Atlantic regions to explain the abrupt warming over Greenland during D-O events, by lowering the albedo and exposing relatively warm surface waters to the cold high-latitude atmosphere (10, 57, 58).

The large-amplitude and high-frequency sea ice fluctuations identified in the NEEM Br_{enr} record during interstadials are previously unresolved features of the glacial D-O events. Similar high-frequency climate oscillations have recently been resolved in European lake records during interstadials, as well as during the Holocene, and linked with an increased Atlantic multidecadal oscillation (59). We surmise that short-term sea ice fluctuations in the Baffin Bay might have been an integral part of an increased degree of North Atlantic climate instability on multidecadal timescales. However, longer and more continuous high-resolution proxy records are needed to unravel the periodicity of these interstadial sea ice fluctuations and ascribe them to a forcing. The reconstructed extensive MYSI in the Baffin Bay and northern Labrador Sea during GS would support the role of an extended sea ice cover in contributing to a change in atmospheric circulation patterns over the North Atlantic that led to a suppression of Atlantic multidecadal climate oscillations in Europe (59).

Finally, the marked increase in Br_{enr} and its variability observed during the mid-to-late phase of GI is indicative of the most extended seasonal sea ice condition in the NEEM aerosols source region. This could be achieved both with an expansion of seasonal sea ice at the expense of perennial sea ice across all of Baffin Bay and/or with an expansion of seasonal sea ice southward of the perennial sea ice edge.

Since we have no direct evidence of sea ice regimes in the Baffin Bay during interstadial periods, none of the hypothesis can be discarded. However, available sea ice reconstructions for the Holocene suggest the presence of a perennial sea ice cover in the central Baffin Bay during the Early Holocene [~9.5 ka (60)], when atmospheric temperatures, sea surface temperatures, and solar insolation were significantly higher than during interstadial climate warmings (24, 60). This, in turn, corroborates the second scenario in which, during GI, a mixture of (reduced-) perennial and seasonal sea ice cover spreads over the northern and central Baffin Bay and events of rapid southward expansion of seasonal sea ice occurred, delayed 0.1–0.6 ky after the D-O onsets (Fig. 5*C*).

Such mid-to-late interstadial seasonal sea ice expansions, also consistent with the GS16-204–23CC biomarker records and modeled sea ice edge position during D-O events (46), could be related to injections of freshwater from the melting of Laurentide and Greenland continental ice masses into the Baffin Bay and the Labrador Sea (32) as a consequence of increased atmospheric temperatures (4, 7, 33). The consequent increase of sea ice export likely led to a freshening of the subpolar North Atlantic through sea ice melting, which would have reduced deep-water formation. The seasonal sea ice expansion and freshening of the subpolar North Atlantic may thus have contributed to a gradual cooling of the North Atlantic preceding the

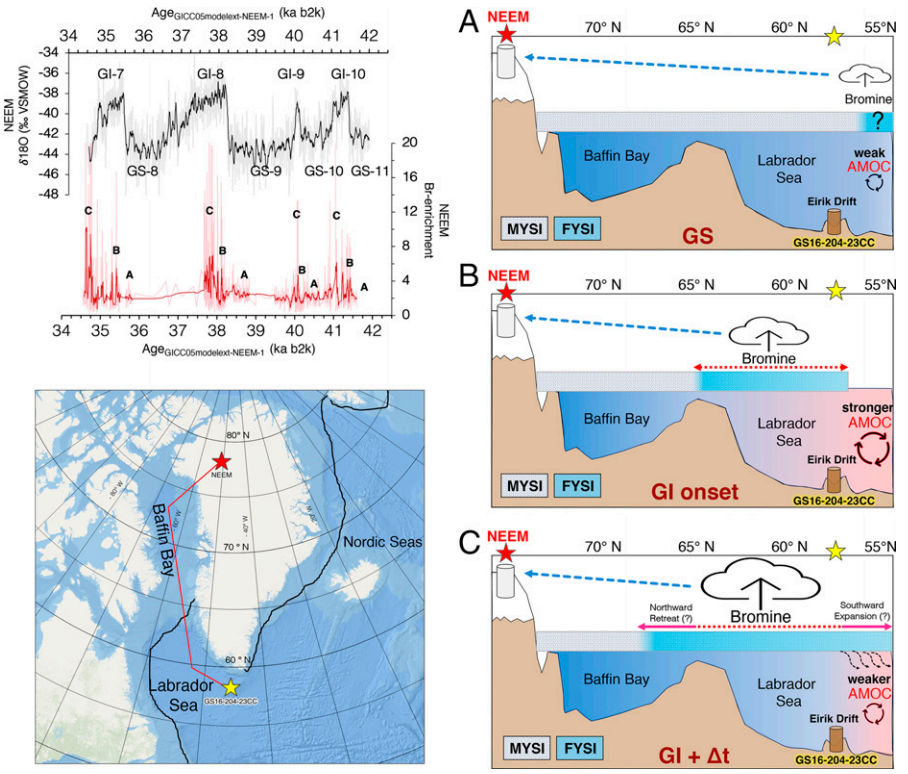

Fig. 5. Sea ice reconstruction of Baffin Bay during D-O cycles 7–10. Looking at NEEM Br_{enr} profile (red curve) between, three distinct stages (*A, B, C*) can be identified for each D-O cycle: (*A*) During GS, a widespread perennial or MYSI cover spreads over Arctic Ocean and in the oceanic regions surrounding Greenland including the Baffin Bay and the Labrador Sea. (*B*) Synchronously or within a decade from the GI onset, the perennial sea ice edge in the Baffin Bay gradually retreats and it is partially substituted by seasonal sea ice conditions. (*C*) During the mid-to-late phase of the GI (~0.1–0.6 ka after the onset), highest Br_{enr} values suggest both a significant retreat of the perennial sea ice edge and/or, more likely, a major FYSI expansion southward into the western North Atlantic. In the latter scenario, the increased ice-albedo feedbacks and the enhanced sea ice export in the Labrador Sea (generating a weakening of the AMOC) culminated at or near the onset of the new stadial phase (*A*).

transition to stadial conditions (61). Once a critical threshold was reached, the gradual cooling and underlying processes would have led to a rapid reduction of deep-water formation and the AMOC, as well as rapid Greenland cooling at the onset of the stadial period (Fig. 5*A*) (62, 63). In this sense, the expansion of an extended FYSI and consequently the build-up of MYSI west and south of Greenland acted as an efficient driver of climate cooling through the ice-albedo feedback, as well as by affecting the North Atlantic ocean circulation.

In conclusion, our results suggest and support that sea ice decline occurred rapidly and synchronously with abrupt high-latitude warming during the D-O events, similarly to what is observed in recent decades in the Arctic region (13, 64). In addition, the seasonal sea ice formation and short-term, large-amplitude fluctuations during the mid-to-late interstadial periods could have played a central role in the subpolar North Atlantic feedback loop that led to a gradual cooling and conditions that would result in a nonlinear, abrupt AMOC reduction and Greenland cooling.

Materials and Methods

Concentrations of Br and Na were determined by Inductively Coupled Plasma Sector Field Mass Spectrometry (ICP-SFMS; Element2, ThermoFischer, Bremen, Germany) equipped with a cyclonic Peltier-cooled spray chamber (ESI, Omaha, USA) (24, 42) (*SI Appendix, Materials and Methods*). High-resolution (0.05 cm) NEEM δ18O analysis were performed with Cavity Ring Down Spectroscopy (CRDS) in the near Infra-Red region (34). The age model of sediment core GS16-204–23CC is based on stratigraphic alignment of marine proxy records and the NEEM δ18O record, using signals in ARM, near-surface temperature, and cryptotephra layers (*SI Appendix, Materials and Methods*). Biomarkers were extracted from freeze-dried and homogenized sediment samples using dichloromethane:methanol (2:1, vol/vol) as solvent, separated into hydrocarbon and sterol fractions, and analyzed by gas chromatography/mass spectrometry. The methodology and the age model of core GS16-204–23CC are detailed in *SI Appendix, Materials and Methods*.

Data, Materials, and Software Availability. Sea ice proxy data from the NEEM ice core and GS16-204-23CC marine core presented in this study have been deposited in Zenodo repository (10.5281/zenodo.7180408) (66). All study data are included in the article and *SI Appendix*.

ACKNOWLEDGMENTS. The research leading to these results has received funding from the European Research Council under the European Union's Seventh Framework Programme (FP7/2007–2013) grant agreements #243908 "Past4Future. Climate change–Learning from the past climate" and #610055 "Ice2ice". We thank our colleagues at *Centre for Ice and Climate* (Copenhagen, Denmark) for their generous contribution and providing the NEEM ice core samples. NEEM is directed and organized by the Center of Ice and Climate at the Niels Bohr Institute and US NSF, Office of Polar Programs. It is supported by funding agencies and institutions in Belgium (FNRS-CFB and FWO), Canada (NRCan/GSC), China (CAS), Denmark (FIST), France (IPEV, CNRS/INSU, CEA and ANR), Germany (AWI), Iceland (RannIs), Japan (NIPR), Korea (KOPRI), The Netherlands (NWO/ALW), Sweden (VR), Switzerland (SNF), United Kingdom (NERC), and the USA (US NSF, Office of Polar Programs).

Author affiliations: [a]Institute of Atmospheric Sciences and Climate - National Research Council of Italy, ISAC-CNR, University Campus Ecotekne, 73100 Lecce (LE), Italy; [b]Department of Environmental Sciences, Informatics and Statistics, Ca' Foscari University of Venice, 30170 Venice, Italy; [c]Marine Geology Section, Alfred Wegener Institute Helmholtz Centre for Polar and Marine Research, 27568 Bremerhaven, Germany; [d]Institute of Polar Sciences - National Research Council of Italy, ISP-CNR, Venezia-Mestre (VE), 30172 Italy; [e]Department of Statistical Sciences, University of Padua, 35121 Padua, Italy; [f]Physics of Ice Climate and Earth, Niels Bohr Institute,

University of Copenhagen, Copenhagen 2200, Denmark; [g]Centre for Earth Observation Science, University of Manitoba, Winnipeg, R3T 2N2 MB, Canada; [h]Paul Scherrer Institute, Laboratory of Environmental Chemistry, 5232 Villigen, PSI, Switzerland; [i]Department of Atmospheric Chemistry and Climate, Institute of Physical Chemistry Rocasolano, CSIC, Madrid, Spain; and [j]MARUM Center for Marine Environmental Sciences and Faculty of Geosciences, University of Bremen, 28334 Bremen, Germany

1. W. Dansgaard *et al.*, Evidence for general instability of past climate from a 250-kyr ice-core record. *Nature* **364**, 218–220 (1993).
2. K. K. Andersen *et al.*; North Greenland Ice Core Project members, High-resolution record of Northern Hemisphere climate extending into the last interglacial period. *Nature* **431**, 147–151 (2004).
3. P. Kindler *et al.*, Temperature reconstruction from 10 to 120 kyr b2k from the NGRIP ice core. *Clim. Past* **10**, 887–902 (2014).
4. M. Guillevic *et al.*, Spatial gradients of temperature, accumulation and δ18O- ice in Greenland over a series of Dansgaard-Oeschger events. *Clim. Past* **9**, 1029–1051 (2013).
5. M. F. Jensen *et al.*, A spatiotemporal reconstruction of sea-surface temperatures in the North Atlantic during Dansgaard-Oeschger events 5-8. *Clim. Past* **14**, 901–922 (2018).
6. T. Erhardt *et al.*, Decadal-scale progression of the onset of Dansgaard-Oeschger warming events. *Clim. Past* **15**, 811–825 (2019).
7. E. Capron *et al.*, The anatomy of past abrupt warmings recorded in Greenland ice. *Nat. Commun.* **12**, 2106 (2021).
8. A. H. Voelker, Global distribution of centennial-scale records for Marine Isotope Stage (MIS) 3: a database. Quat. Sci. Rev. **21**, 1185–1212 (2002).
9. H. Sadatzki *et al.*, Sea ice variability in the southern Norwegian Sea during glacial Dansgaard-Oeschger climate cycles. *Sci. Adv.* **5**, eaau6174 (2019).
10. H. Sadatzki *et al.*, Rapid reductions and millennial-scale variability in Nordic Seas sea ice cover during abrupt glacial climate changes. *Proc. Natl. Acad. Sci. U.S.A.* **117**, 29478–29486 (2020).
11. P. Vallelonga *et al.*, Sea-ice-related halogen enrichment at Law Dome, coastal East Antarctica. *Clim. Past* **13**, 171–184 (2017).
12. A. Dai, D. Luo, M. Song, J. Liu, Arctic amplification is caused by sea-ice loss under increasing CO_2. *Nat. Commun.* **10**, 121 (2019).
13. M. C. Serreze, R. G. Barry, Processes and impacts of Arctic amplification: A research synthesis. *Global Planet. Change* **77**, 85–96 (2011).
14. A. De Vernal, R. Gersonde, H. Goosse, M. S. Seidenkrantz, E. W. Wolff, Sea ice in the paleoclimate system: The challenge of reconstructing sea ice from proxies - an introduction. *Quat. Sci. Rev.* **79**, 1–8 (2013).
15. C. Kinnard *et al.*, Reconstructed changes in Arctic sea ice over the past 1,450 years. *Nature* **479**, 509–512 (2011).
16. N. J. Abram, E. W. Wolff, M. A. Curran, A review of sea ice proxy information from polar ice cores. Quat. Sci. Rev. **79**, 168–183 (2013).
17. S. T. Belt, G. Massé, S. J. Rowland, M. Poulin, C. Michel, B. LeBlanc, A novel chemical fossil of palaeo sea ice: IP25. *Org. Geochem.* **38**, 16–27 (2007).
18. J. K. Volkman, A review of sterol markers for marine and terrigenous organic matter. *Org. Geochem.* **9**, 83–99 (1986).
19. L. Smik, P. Cabedo-Sanz, S. T. Belt, Semi-quantitative estimates of paleo Arctic sea ice concentration based on source-specific highly branched isoprenoid alkenes: A further development of the PIP25 index. *Org. Geochem.* **92**, 63–69 (2016).
20. S. T. Belt *et al.*, Identification of paleo Arctic winter sea ice limits and the marginal ice zone: Optimised biomarker-based reconstructions of late Quaternary Arctic sea ice. *Earth Planet. Sci. Lett.* **431**, 127–139 (2015).
21. P. Vallelonga *et al.*, Sea-ice reconstructions from bromine and iodine in ice cores. *Quat. Sci. Rev.* **269**, 107133 (2021).
22. N. Maffezzoli *et al.*, A 120,000-year record of sea ice in the North Atlantic? *Clim. Past* **15**, 2031–2051 (2019).
23. U. Hoff, T. L. Rasmussen, R. Stein, M. M. Ezat, K. Fahl, Sea ice and millennial-scale climate variability in the Nordic seas 90 kyr ago to present. *Nat. Commun.* **7**, 12247 (2016).
24. A. Spolaor *et al.*, Canadian Arctic sea ice reconstructed from bromine in the Greenland NEEM ice core. *Sci. Rep.* **6**, 33925 (2016).
25. NEEM community members, Eemian interglacial reconstructed from a Greenland folded ice core. *Nature* **493**, 489–494 (2013).
26. S. O. Rasmussen *et al.*, A first chronology for the North Greenland Eemian Ice Drilling (NEEM) ice core. *Clim. Past* **9**, 2713–2730 (2013).
27. L. A. Barrie *et al.*, Arctic contaminants: Sources, occurrence and pathways. *Sci. Total Environ.* **122**, 1–74 (1992).
28. M. A. Tschudi, W. N. Meier, J. S. Stewart, C. Fowler, J. Maslanik, EASE-Grid Sea Ice Age, Version 4. Boulder Colorado USA. NASA National Snow and Ice Data Center Distributed Active Archive Center. https:/doi.org/https://doi.org/10.5067/UTAV7490FEPB. Accessed 1 July 2020.
29. W. R. Peltier, Ice age paleotopography. *Science* **265**, 195–201 (1994).
30. P. Slabon *et al.*, Greenland ice sheet retreat history in the northeast Baffin Bay based on high-resolution bathymetry. *Quat. Sci. Rev.* **154**, 182–198 (2016).
31. E. Brouard, P. Lajeunesse, Maximum extent and decay of the Laurentide Ice Sheet in Western Baffin Bay during the Last glacial episode. *Sci. Rep.* **7**, 10711 (2017).
32. E. J. Gowan *et al.*, A new global ice sheet reconstruction for the past 80 000 years. *Nat. Commun.* **12**, 1199 (2021).
33. M. S. Seidenkrantz *et al.*, Southwest Greenland shelf glaciation during MIS 4 more extensive than during the Last Glacial Maximum. *Sci. Rep.* **9**, 15617 (2019).
34. V. Gkinis *et al.*, A 120,000-year long climate record from a NW-Greenland deep ice core at ultra-high resolution. *Sci. Data* **8**, 141 (2021).
35. W. F. Ruddiman, Late Quaternary deposition of ice-rafted sand in the subpolar North Atlantic (lat 40° to 65°N). *Bull. Geol. Soc. Am.* **88**, 11813 (1977).
36. S. Schüpbach *et al.*, Greenland records of aerosol source and atmospheric lifetime changes from the Eemian to the Holocene. *Nat. Commun.* **9**, 1476 (2018).
37. F. J. Millero, R. Feistel, D. G. Wright, T. J. McDougall, The composition of Standard Seawater and the definition of the Reference-Composition Salinity Scale. *Deep Sea Res. Part I: Oceanogr. Res. Pap.* **55**, 50–72 (2008).
38. R. Vogt, P. J. Crutzen, R. Sander, A mechanism for halogen release from sea-salt aerosol in the remote marine boundary layer. *Nature* **383**, 327–330 (1996).
39. T. Wagner, U. Platt, Observation of tropospheric BrO from the GOME satellite. *Nature* **395**, 486–490 (1998).
40. I. Bougoudis *et al.*, Long-term time series of Arctic tropospheric BrO derived from UV–VIS satellite remote sensing and its relation to first-year sea ice. *Atmos. Chem. Phys.* **20**, 11869–11892 (2020).
41. A. Spolaor *et al.*, Halogen species record Antarctic sea ice extent over glacial-interglacial periods. *Atmos. Chem. Phys.* **13**, 6623–6635 (2013).
42. A. Spolaor *et al.*, Seasonality of halogen deposition in polar snow and ice. *Atmos. Chem. Phys.* **14**, 9613–9622 (2014).
43. A. Spolaor *et al.*, Halogen-based reconstruction of Russian Arctic sea ice area from the Akademii Nauk ice core (Severnaya Zemlya). *Cryosphere* **10**, 245–256 (2016).
44. A. Saiz-Lopez, R. von Glasow, Reactive halogen chemistry in the troposphere. *Chem. Soc. Rev.* **41**, 6448–6472 (2012).
45. W. R. Simpson *et al.*, First-year sea-ice contact predicts bromine monoxide (BrO) levels at Barrow, Alaska better than potential frost flower contact. *Atmos. Chem. Phys.* (2007).
46. L. C. Sime, P. O. Hopcroft, R. H. Rhodes, Impact of abrupt sea ice loss on Greenland water isotopes during the last glacial period. *Proc. Natl. Acad. Sci. U.S.A.* **116**, 4099–4104 (2019).
47. M. Zheng *et al.*, Climate information preserved in seasonal water isotope at NEEM: relationships with temperature, circulation and sea ice. *Clim. Past* **14**, 1067–1078 (2018).
48. A. H. Voelker, H. Haflidason, Refining the Icelandic tephrachronology of the last glacial period – The deep-sea core PS2644 record from the southern Greenland Sea. *Global and Planetary Change* **131**, 35–62 (2015).
49. E. R. Thomas, R. Mulvaney, E. W. Wolff, A change in seasonality in Greenland during a Dansgaard-Oeschger warming. *Ann. Glaciol.* **48**, 19–24 (2008).
50. G. Krinner, C. Genthon, J. Jouzel, GCM analysis of local influences on ice core δ signals. *Geophys. Res. Lett.* **24**, 2825–2828 (1997).
51. S. O. Rasmussen *et al.*, A stratigraphic framework for abrupt climatic changes during the Last Glacial period based on three synchronized Greenland ice-core records: Refining and extending the INTIMATE event stratigraphy. *Quat. Sci. Rev.* **106**, 14–28 (2014).
52. J. Müller *et al.*, Towards quantitative sea ice reconstructions in the northern North Atlantic: A combined biomarker and numerical modelling approach. *Earth Planet. Sci. Lett.* **306**, 137–148 (2011).
53. H. M. Kolling *et al.*, Biomarker Distributions in (Sub)-Arctic Surface Sediments and Their Potential for Sea Ice Reconstructions. *Geochem. Geophys. Geosyst.* **21**, 1–28 (2020).
54. L. Henry *et al.*, North Atlantic ocean circulation and abrupt climate change during the last glaciation. *Science* **353**, 470–474 (2016).
55. S. Van Kreveld *et al.*, Potential links between surging ice sheets, circulation changes, and the Dansgaard-Oeschger cycles in the Irmiger Sea, 60-80 kyr. *Paleoceanography* **15**, 425–442 (2000).
56. G. Vettoretti, W. R. Peltier, Thermohaline instability and the formation of glacial North Atlantic super polynyas at the onset of Dansgaard-Oeschger warming events. *Geophys. Res. Lett.* **43**, 5336–5344 (2016).
57. C. Li, D. S. Battisti, C. M. Bitz, Can North Atlantic sea ice anomalies account for Dansgaard-Oeschger climate signals? *J. Clim.* **23**, 5457–5475 (2010).
58. C. Li, A. Born, Coupled atmosphere-ice-ocean dynamics in Dansgaard-Oeschger events. *Quat. Sci. Rev.* **203**, 1–20 (2019).
59. F. Sirocko *et al.*, Muted multidecadal climate variability in central Europe during cold stadial periods. *Nat. Geosci.* **14**, 651–658 (2021).
60. O. T. Gibb, S. Steinhauer, B. Fréchette, A. De Vernal, C. Hillaire-Marcel, Diachronous evolution of sea surface conditions in the Labrador Sea and Baffin Bay since the last deglaciation. *The Holocene* **25**, 1882–1897 (2015).
61. S. Barker *et al.*, Icebergs not the trigger for North Atlantic cold events. *Nature* **520**, 333–336 (2015).
62. W. S. Broecker, G. Bond, M. Klas, G. Bonani, W. Wolfli, A salt oscillator in the glacial Atlantic? 1. The concept. *Paleoceanography* **5**, 469–477 (1990).
63. J. B. Pedro *et al.*, Beyond the bipolar seesaw: Toward a process understanding of interhemispheric coupling. *Quat. Sci. Rev.* **192**, 27–46 (2018).
64. E. Jansen *et al.*, Past perspectives on the present era of abrupt Arctic climate change. *Nat. Clim. Chang.* **10**, 714–721 (2020).
65. F. Fetterer, K. Knowles, W. N. Meier, *Sea Ice Index, Version 3* (National Snow and Ice Data Center, 2017).
66. F. Scoto *et al.*, Sea ice proxy data from "Sea ice fluctuations in the Baffin Bay and the Labrador Sea during glacial abrupt climate changes". Zenodo. https://zenodo.org/record/7180408#.Y0mdbUxByUk. Deposited 11 October 2022.